Liver stiffness assessment with tagged MRI of cardiac-induced liver motion in cirrhotic patients

Sohae Chung, PhD[1], **Kyoung-Eun Kim, MD**[2], **Mi-Suk Park, MD**[2], **Sharath Bhagavatula, BS**[1], **James Babb, PhD**[1], and **Leon Axel, PhD, MD**[1]

[1]Center for Biomedical Imaging, Radiology Department, New York University Langone Medical Center, New York, NY 10016, USA

[2]Department of Diagnostic Radiology, Severance Hospital, Yonsei University College of Medicine, Seodaemum-Gu, Seoul 120-752, South Korea

Abstract

Purpose—To assess liver stiffness by using magnetization-tagged MRI to measure the cardiac-induced motion in the liver of cirrhosis patients with known Child-Pugh scores.

Materials and Methods—Tagged MRI was performed using a 3T MR scanner on 52 cirrhosis patients classified into 2 groups: liver cirrhosis with Child-Pugh A (LCA;n=39) and liver cirrhosis with Child-Pugh B or C (LCBC;n=13). We also included 19 healthy controls. Tagged images were acquired encompassing both the liver and the heart. The corresponding displacement and strains were calculated using a Gabor filter bank. The maximum displacement (MaxDisp) was found over the cardiac cycle, as well as the local maximum P1 (MaxP1) and minimum P2 strains (MinP2). Group comparisons were made without and with adjustment for age and gender.

Results—In control, LCA, and LCBC groups, the MaxDisp was 3.98±0.88 mm, 2.52±0.73 mm, and 1.86±0.77 mm; the MaxP1 was 0.10±0.02, 0.04±0.01, and 0.02±0.01; and the MinP2 was −0.08±0.01, −0.05±0.02, and −0.03±0.01, respectively. Statistically significant differences were found between groups (p<0.05 for all).

Conclusion—This method measures cardiac-induced liver motion and deformation to assess liver stiffness. Significant differences were found in our stiffness measures between control, LCA, and LCBC groups, with more severe disease being associated with greater stiffness.

Keywords

magnetization-tagged MRI; liver stiffness; cardiac-induced liver motion; Child-Pugh score; cirrhosis

INTRODUCTION

Liver fibrosis refers to the accumulation of excess fibrous tissue in the liver; progressive fibrosis can lead to cirrhosis. Liver fibrosis is generally considered to be irreversible in its advanced stages. However, there is increasing evidence of better reversibility of liver fibrosis (1–3). Furthermore, fibrosis may serve as a marker of the presence of progressive liver disease while it is still in a subclinical and more treatable state. Therefore, it is very important to know the fibrosis stage for the most effective treatment of liver disease, and for

Please send correspondence to: Leon Axel, PhD, MD, Center for Biomedical Imaging, Department of Radiology, New York University Langone Medical Center, 660 First Avenue, Room 411, New York, NY 10016, leon.axel@nyumc.org, Telephone: 212-263-6248, Fax: 212-263-7541.

the prevention of later complications of liver disease, such as liver failure, variceal bleeding, hepatocellular carcinoma, etc.

Liver biopsy is currently considered the gold standard for assessing fibrosis. However, it is invasive and potentially risky for the patient. Moreover, the accuracy of liver biopsy remains limited because of the potential for sampling and observation errors (4, 5). Thus, there is a need to develop and validate noninvasive methods to assess liver fibrosis. Ultrasound-based transient elastography, using special-purpose ultrasound systems, has been shown to be a reliable noninvasive method to stage liver fibrosis, based on the observation that fibrosis leads to increased mechanical stiffness of the liver (6–8). Magnetic resonance (MR) elastography has emerged as a relatively new imaging technique, which observes propagating shear waves induced by an external vibration source (9, 10), with an increased stiffness resulting in increased propagation speed; many studies have shown its feasibility for staging liver fibrosis (11–13). However, it requires special-purpose hardware in order to generate the external vibrations and to synchronize them with the imaging. As an alternative to the use of external sources of force applied to the liver in order to assess its stiffness, recent studies have shown that intrinsic internal body motions can be used, together with magnetization-tagged MRI (14), to measure the respiratory-induced motion of the liver (15) or the cardiac-induced motion of the liver (16); fibrotic livers show different patterns of motion and deformation than normal livers, due to their increased stiffness. While respiratory motion can affect a relatively larger portion of the liver, the cardiac-induced motion of the liver is mainly found in the area underneath the heart. However, patient cooperation is required for generating the respiratory-induced motion of the liver in a controlled way for imaging, so that they exhale on command at a constant speed from maximal inspiratory to maximal expiratory phases. Furthermore, additional motion correction should generally be performed with respiratory approaches, due to possible changes in body position caused by respiratory motion, while this issue may be less important with the use of cardiac pulsation, because of breath-holding by subjects during imaging; these respiratory motion corrections can be subject to some intra- or inter-subjective variability. Therefore, we have used the cardiac pulsation as an intrinsic motion source to transiently deform the liver.

In this study, we have assessed liver stiffness by using magnetization-tagged MRI to measure the cardiac-induced motion and deformation in the liver in cirrhotic patients and normal controls. Although the Child-Pugh score is not directly a fibrosis score but rather a prognostic score, previous studies have shown that liver stiffness correlates well with Child-Pugh score in patients with cirrhosis (17, 18). Based on those findings, we included only patients with cirrhosis, and aimed to assess the potential utility of our method by comparing our stiffness measures in a healthy control group and in two cirrhotic patient groups, stratified by Child-Pugh scores. We hypothesized that our stiffness measures can differentiate patients with earlier stages of cirrhosis from both later stages and control subjects.

MATERIALS AND METHODS

Study Population

Between April 2010 and July 2010, tagged MR images were acquired from 52 patients with liver cirrhosis (mean age, 59.3 ± 9.5 years old; age range, 40 – 80 years). 19 control subjects with no significant medical history or clinical signs of liver disease (mean age, 29.4 ± 5.2 years old; age range, 22 – 43 years) were also included in the study (Table 1). Potential subjects were excluded from this study if there was a history of known heart disease (4 patients) or if there was insufficient MR image quality for analysis (9 patients), e.g., due to having respiratory motion during imaging, short left lobe of liver (with too little overlap

with the heart for motion assessment), or severe ascites (but, patients with mild ascites were included in the study (12 patients)). Protocols of the human studies were approved by our institutional review board and informed consent was obtained from all participants. Patients with liver cirrhosis were classified into 2 groups based on their Child-Pugh score: 1) liver cirrhosis with Child-Pugh A (LCA; n = 39) (mean age, 58.4 ± 9.6 years old; mean Child-Pugh score, 5.1 ± 0.3); and 2) liver cirrhosis with Child-Pugh B (n = 11) or C (n = 2) (LCBC) (mean age, 62 ± 9.1 years old; mean Child-Pugh score, 7.8 ± 1.1). The liver disease etiology in the LCA patient group included hepatitis B virus (HBV) (n = 28), hepatitis C virus (HCV) (n = 6), dual hepatitis B and C virus (B+C) (n = 2), and non-B non-C hepatitis (NBNC) (n = 3). The etiology in the LCBC patient group included HBV (n = 8), HCV (n = 2), NBNC (n = 2), and alcohol abuse (n = 1).

MR Imaging

Tagged MR images were obtained before routine liver MR imaging using a 3T whole-body MR scanner (Tim Trio; Siemens Medical Solutions, Erlangen, Germany) with standard phased-array coils. A conventional electrocardiogram-gated spatial modulation of magnetization (SPAMM) imaging sequence with two-dimensional grid tags (14) (triggered at the beginning of systole) was performed covering the cardiac cycle, with breadth-holding by the subjects. Imaging parameters included: echo time = 3.9 msec, repetition time = 8.0 msec, temporal resolution = 48.2 msec, flip angle = 10°, field of view = 300 mm × 300 mm, matrix = 256 × 174, in-plane resolution = 1.2 mm × 1.7 mm, slice thickness = 6 mm, tag thickness = 1.5 mm, tag spacing = 7 mm, tag orientation = ± 45°, receiver bandwidth = 201 Hz/pixel, and generalized autocalibrating partially parallel acquisitions (GRAPPA) acceleration factor 2 with 24 reference k-space lines. Tagged images were acquired in 3 coronal and 3 sagittal planes encompassing both the liver and the heart (Figure 1). Total image acquisition time per slice was approximately 15 – 20 sec.

Image and Data Analyses

A Gabor filter bank was used to automatically track the tags, in order to measure the displacement and strains within the liver adjacent to the heart in the tagged MR images (16), using custom software developed in MATLAB R2010b (The MathWorks Inc., MA, USA), and implemented in the Fourier domain. A total of 9 filters with three adjustable parameters (magnitude of the center frequency, orientation, and extent of the Gaussian function) were applied to detect the local tag spacing and orientation within the image, by covering the first harmonic peaks of each quasi-periodic family of tags in the corresponding Fourier domain. Then, two families of phase images, corresponding to the local positions of the vertical and horizontal tag patterns, were computed and the associated displacement field maps were calculated from the unwrapped phase images. The corresponding first principal (P1) and the second principal (P2) strains were calculated from the displacement fields (Figure 2). The P1 and P2 strains represent the amount of the greatest elongation (or lengthening) and compression (or shortening) of the tissue, respectively.

Regions of interest (ROI) (approximately 18 mm × 18 mm or 240 pixels) were chosen in liver regions just below the diaphragm, where the greatest displacement and strain values occurred. The local maximum displacement (MaxDisp) (mm), the local maximum P1 strain (MaxP1), and the local minimum P2 strain (MinP2) were found from among the results of the six imaging planes over the whole cardiac cycle. Note that positive strain values represent elongation and negative values indicate compression. Therefore, the greatest absolute value occurs at the maximum in P1 strain, but at the minimum (negative value) in P2 strain. The image analysis was performed in blinded fashion by a trained expert.

Statistical Analysis

Analysis of variance and covariance were used to compare subject groups in terms of each measure without and with adjustment for age and gender. Age and gender were included in a multivariable binary logistic regression model which assessed the utility of imaging measures, alone or in combination, as predictors of cirrhosis adjusted for age and gender. In all analyses, the error variance was allowed to differ across comparison groups to remove the assumption of variance homogeneity and a Shapiro-Wilk test applied to the residuals from each model was used to validate the underlying assumption of normality. All statistical tests were conducted at the two-sided 5% significance level, but p-values are also reported with a Tukey's Honest Significant Difference (HSD) multiple comparison correction for unequal group size. The data are given as mean ± standard deviation (SD). Binary logistic regression and receiver operating characteristic (ROC) curve analyses were used to evaluate the utility of the stiffness measures for prediction of Child-Pugh A or greater and Child-Pugh B or greater. Binary logistic regression was used to identify sets of independent predictors of group membership. The logistic model fit to each selected set of factors computes the predicted probability that a subject has cirrhosis given the data observed for that subject. This predicted probability was used as the test criterion in an ROC analysis to assess the diagnostic utility of measures used in combination as predictors of cirrhosis. SAS 9.3 software (SAS Institute, Cary, NC, USA) and SPSS 19.0 software package (SPSS Inc., Chicago, IL, USA) were used for statistical analysis. Statistical analysis was supervised by an expert biostatistician.

RESULTS

Figure 2 shows coronal tagged MR images of a representative control subject and a LCBC patient, with the corresponding absolute displacement and P1/P2 strain color-maps superimposed over the liver. In the control subject, relatively greater deformation is seen to be localized below the heart, but the deformation is qualitatively less pronounced and less locally concentrated in the LCBC patient. This reflects higher resistance to deformation in the cirrhotic liver.

The boxplots of the results for the three groups are presented in Figure 3. There were significant differences between all groups for the MaxDisp (3.98 ± 0.88 mm, 2.52 ± 0.73 mm, and 1.86 ± 0.77 mm for the control group, LCA patient group and LCBC patient group, respectively; $p < 0.0001$ to 0.0079; HSD adjusted $p < 0.0001$ to 0.0214) (Fig. 3a). The MaxP1 (0.1 ± 0.02) for the control group was significantly higher than for the LCA patient group (0.04 ± 0.01) ($p < 0.0001$; HSD adjusted $p < 0.0001$) and the LCA group was also significantly different from the LCBC patient group (0.02 ± 0.01) ($p < 0.0001$; HSD adjusted $p < 0.0001$) (Fig. 3b). The MinP2 values for the control group, LCA patient group, and LCBC patient group (−0.08 ± 0.01, −0.05 ± 0.02, −0.03 ± 0.01, respectively) were also all significantly different ($p < 0.0001$; HSD adjusted $p < 0.0001$) (Fig. 3c). After adjustment for age and gender, p-values ranged from < 0.0001 to 0.0071 and HSD adjusted p-values ranged from < 0.0001 to 0.0349. The stiffness measures and p-values are summarized in Table 2 and Table 3, respectively.

Using ROC analysis, we found our stiffness measures to be a significant predictor of Child-Pugh A or greater and of Child-Pugh B or greater (Table 4), both separately and together; corresponding ROC curves were shown in Figure 4. Briefly, for prediction of Child A or greater with all stiffness measures, we found an area under the curve (AUC) of 0.998 with a sensitivity of 98.1% and specificity of 94.7%. For prediction of Child B or greater with all stiffness measures, we found an AUC of 0.934 with a sensitivity of 92.3% and specificity of 87.9%.

DISCUSSION

This study has evaluated the ability to assess liver stiffness by using tagged MRI to measure cardiac-induced liver motion and deformation, and has found statistically significant differences in our stiffness measures between control subjects and cirrhosis patients, and between cirrhosis patient groups with different severity of disease classified by the Child-Pugh score. High sensitivity and specificity were found in our stiffness measures for prediction of Child-Pugh A or greater and of Child-Pugh B or greater. Therefore, this method has the potential to be used for noninvasive detection of early-stage (or well-compensated) liver cirrhosis, potentially allowing earlier diagnosis and the potential of more effective treatment in its earlier stage. In addition, this method has the potential to be used for identifying patients that will have a more rapid progression of cirrhosis and the development of clinical decompensation, for their effective treatment. Our initial results are encouraging enough that undertaking future longitudinal studies (of patients with initially well-compensated cirrhosis) seems warranted.

In this study, we performed conventional tagged MRI with a 3T MR scanner. Since the tags can persist for times on the order of the longitudinal relaxation time (T_1) of the tissue, they can be more clearly seen at 3T than 1.5T, due to greater persistence through the cardiac cycle. However, a previous study (16) has also shown its feasibility on 1.5T, since tags can persist until mid-diastole in most patients at 1.5T and the greatest values of our measures occur during end-systole (~300ms, which is less than a typical liver T_1 of approximately 600ms (19) at 1.5T). In addition, all tagged MR imaging studies were performed before injection of any T_1-shortening contrast agents that were used in the associated routine clinical liver MRI examination, to maximize the tag persistence.

This method provides a novel set of MR image-derived measures related to liver stiffness, which can be acquired without the need for any special-purpose hardware for externally producing liver motion, by assessing the natural cardiac-induced motion of the liver. As shown in a previous study (15), the respiratory motion of the liver can also be used to assess liver stiffness; it has the relative advantage of affecting a relatively larger portion of the liver. However, patient cooperation, such as exhaling at a constant speed from maximal inspiratory to maximal expiratory phases and in a way that is synchronized with the imaging, is generally required for generating the respiratory-induced motion of the liver in a controlled way for imaging. This can cause possible changes in body position and can also be subject to some intra- or inter-subjective variability. These issues may be less important for our proposed method using cardiac pulsation, because of breath-holding by subjects during imaging, no other actions are required of the patient. Therefore, it could be readily and easily implemented on any conventional MRI systems with cardiac imaging capabilities.

In a recent study, Mannelli et al (20) compared a small number of control subjects to cirrhotic patients using a similar technique and also showed statistically significant differences between groups. They also performed tagged MRI to measure cardiac-induced liver motion, but using a peripheral pulse-triggering method instead of using electrocardiogram-triggering. While electrocardiogram-gated imaging primarily focuses on the cardiac-contraction-induced or "pull-up" deformation in the liver during systole, peripheral pulse-gated imaging has a typical delay relative to electrocardiogram-triggering, so that we primarily observe cardiac-relaxation-induced or "let-down" deformation in the liver during diastole with such an approach. It would be interesting to compare the effects of these two different motion mechanisms in the liver in further studies.

This method can be complementary to other methods, such as ultrasound-based elastography or MR elastography, since cardiac pulsation is mainly transmitted to the left lobe of the

liver, whereas the other methods primarily approach the right lobe of the liver and may have some difficulties to approach the left lobe, due to the local anatomy and cardiac pulsatility artifact. Our method also works in a different effective frequency range. According to Ozcan et al (21), the storage and loss moduli of human livers increase with an increase in excitation frequency. Thus, this method may provide additional new information on the properties of the liver by using much lower frequency of ~1Hz, compared other more conventional imaging approaches, using frequencies of ~50 Hz for US elastography and of ~65 Hz for MRE. Future work could include combining this method with other methods to provide a potentially better assessment of liver stiffness.

The present study has certain limitations. First, we could not obtain the histopathologic fibrosis grade as the reference standard in most of the subjects, and so included only cirrhotic patients with known Child-Pugh scores in this study. Although Child-Pugh score is not a fibrosis score itself, previous studies (17–18) have shown that liver stiffness correlates with Child-Pugh score in patients with cirrhosis. Based on those findings, we performed this method only on patients with clinically known cirrhosis, and classified them by their Child-Pugh scores for comparison. Future studies should include further evaluation in patients with a biopsy-proven level of fibrosis; our initial results are sufficiently encouraging that such additional studies seem warranted. Second, the study population was relatively small. The results observed in this study need to be confirmed using a larger patient population. In particular, there is a relative lack of data from age-matched healthy controls. However, analysis of variance and covariance was performed with adjustment for age and gender, and still showed significant p-values (< 0.0001 to 0.0071) and HSD adjusted p-values (< 0.0001 to 0.0349) when comparing groups. Third, this method may have some potential problems if applied to subjects with large amounts of ascites, pericardial effusions, systolic heart failure or a short left lobe of liver, because the cardiac motion may not be well transmitted to the liver in such cases. In addition, image quality may be degraded in patients with arrhythmias. In this study, we avoided such possibilities by excluding patients who have known heart disease or severe ascites. However, we found significant differences between control subjects and cirrhotic patients, even with the inclusion of patients with mild ascites. To try to account for variations in the degree of cardiac motion and the heart/liver anatomical coupling among subjects, a measure of the overall displacement could be used to normalize the P1/P2 strains, as shown in a previous study (16). However, since the displacement measured within the liver can be affected by both the cardiac motion and the condition of liver stiffness, the component of liver deformation due to the actual amount of cardiac motion transmitted to the liver could be underestimated due to the correlation between displacement and strain changes, particularly in the patients with stiffer livers. Therefore, such a displacement normalization scheme could reduce apparent relative differences between groups, due to overestimation of the final motion results in the stiffer livers. Further work exploring other, more effective, normalization schemes may be necessary to better discriminate patients with larger ranges of stages of liver fibrosis and different amounts of cardiac- induced motion. Fourth, evaluation of intraobserver and interobserver reproducibility will require further study. We made use of automatic image analysis for calculating displacement and strain maps, which should eliminate much potential user subjectivity and variability. However, the ROIs were selected by an expert observer, and the potential associated intraobserver and interobserver variability was not tested in this study. Future study should investigate such potential variations in our stiffness measures.

In conclusion, this noninvasive method of using cardiac-synchronized tagged MRI for assessing liver stiffness has the potential to replace some liver biopsies, which could be especially useful for longitudinal examinations to monitor progression of disease, as there are significant differences seen between groups with different clinical severity, and it has a high sensitivity and specificity for prediction of Child-Pugh A or greater and Child-Pugh B

or greater in cirrhotic patients. Since it could be implemented on almost any conventional MRI systems, without the need for any special-purpose hardware, by using intrinsic heart motion as the source of induced liver motion, this method could be readily and easily incorporated in routine liver MRI examinations to provide additional information on the state of the liver. Future work would include further validation on patients with a range of degrees of biopsy-proven fibrosis, and a comparison of them with more fully age-matched control subjects, as well as performing longitudinal studies to test the potential of this approach to assess prognosis.

Acknowledgments

References

1. Poynard T, McHutchison J, Davis GL, et al. Impact of interferon alfa-2b and ribavirin on progression of liver fibrosis in patients with chronic hepatitis C. Hepatology. 2000; 32(5):1131–1137. [PubMed: 11050066]

2. Dufour JF, DeLellis R, Kaplan MM. Reversibility of hepatic fibrosis in autoimmune hepatitis. Annals of Internal Medicine. 1997; 127(11):981–985. [PubMed: 9412303]

3. Friedman SL, Bansal MB. Reversal of hepatic fibrosis - Fact or fantasy? Hepatology. 2006; 43(2):S82–S88. [PubMed: 16447275]

4. Holund B, Poulsen H, Schlichting P. Reproducibility of liver-biopsy diagnosis in relation to the size of the specimen. Scandinavian Journal of Gastroenterology. 1980; 15(3):329–335. [PubMed: 7433892]

5. Regev A, Berho M, Jeffers LJ, et al. Sampling error and intraobserver variation in liver biopsy in patients with chronic HCV infection. American Journal of Gastroenterology. 2002; 97(10):2614–2618. [PubMed: 12385448]

6. Ziol M, Handra-Luca A, Kettaneh A, et al. Noninvasive assessment of liver fibrosis by measurement of stiffness in patients with chronic hepatitis C. Hepatology. 2005; 41(1):48–54. [PubMed: 15690481]

7. Yeh WC, Li PC, Jeng YM, et al. Elastic modulus measurements of human liver and correlation with pathology. Ultrasound in Medicine and Biology. 2002; 28(4):467–474. [PubMed: 12049960]

8. Sandrin L, Fourquet B, Hasquenoph JM, et al. Transient elastography: A new noninvasive method for assessment of hepatic fibrosis. Ultrasound in Medicine and Biology. 2003; 29(12):1705–1713. [PubMed: 14698338]

9. Muthupillai R, Lomas DJ, Rossman PJ, Greenleaf JF, Manduca A, Ehman RL. Magnetic-resonance elastography by direct visualization of propagating acoustic strain waves. Science. 1995; 269(5232):1854–1857. [PubMed: 7569924]

10. Yin M, Talwalkar JA, Glaser KJ, et al. Assessment of hepatic fibrosis with magnetic resonance elastography. Clinical Gastroenterology and Hepatology. 2007; 5(10):1207–1213. [PubMed: 17916548]

11. Huwart L, Peeters F, Sinkus R, et al. Liver fibrosis: non-invasive assessment with MR elastography. Nmr Biomed. 2006; 19(2):173–179. [PubMed: 16521091]

12. Huwart L, Sempoux C, Vicaut E, et al. Magnetic resonance elastography for the noninvasive staging of liver fibrosis. Gastroenterology. 2008; 135(1):32–40. [PubMed: 18471441]

13. Rouviere O, Yin M, Dresner MA, et al. MR elastography of the liver: Preliminary results. Radiology. 2006; 240(2):440–448. [PubMed: 16864671]

14. Axel L, Dougherty L. MR imaging of motion with spatial modulation of magnetization. Radiology. 1989; 171(3):841–845. [PubMed: 2717762]

15. Watanabe H, Kanematsu M, Kitagawa T, et al. MR elastography of the liver at 3 T with cine-tagging and bending energy analysis: preliminary results. European Radiology. 2010; 20(10):2381–2389. [PubMed: 20440504]

16. Chung SH, Breton E, Mannelli L, Axel L. Liver stiffness assessment by tagged MRI of cardiac-induced liver motion. Magnet Reson Med. 2011; 65(4):949–955.

17. Foucher J, Chanteloup E, Vergniol J, et al. Diagnosis of cirrhosis by transient elastography (FibroScan): a prospective study. Gut. 2006; 55(3):403–408. [PubMed: 16020491]

18. Recio E, Macias J, Rivero-Juarez A, et al. Liver stiffness correlates with Child-Pugh-Turcotte and MELD scores in HIV/hepatitis C virus-coinfected patients with cirrhosis. Liver Int. 2012; 32(6): 1031–1032. [PubMed: 22405076]

19. Stanisz GJ, Odrobina EE, Pun J, et al. T-1, T-2 relaxation and magnetization transfer in tissue at 3T. Magnet Reson Med. 2005; 54(3):507–512.

20. Mannelli L, Wilson GJ, Dubinsky TJ, et al. Assessment of the liver strain among cirrhotic and normal livers using tagged MRI. J Magn Reson Imaging. 2012; 36(6):1490–1495. [PubMed: 22777877]

21. Umut Ozcan M, Ocal S, Basdogan C, Dogusoy G, Tokat Y. Characterization of frequency-dependent material properties of human liver and its pathologies using an impact hammer. Med Image Anal. 2011; 15(1):45–52. [PubMed: 20655273]
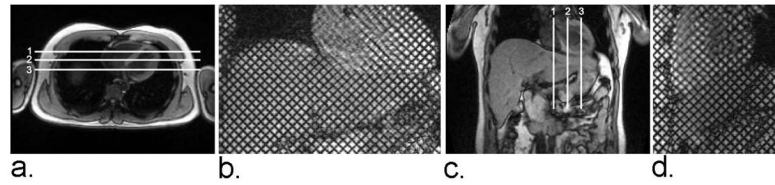
Figure 1.
(a) Axial localizer image showing locations of three coronal imaging planes. (b) Representative coronal end-diastolic grid-tagged MR image. (c) Coronal localizer image showing locations of three sagittal imaging planes. (d) Representative sagittal end-diastolic grid-tagged MR image.
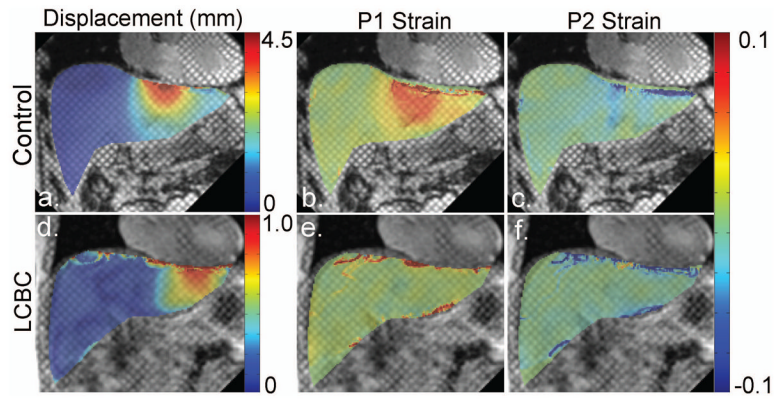
Figure 2.
Representative grid-tagged MR images with superimposed color-coded corresponding displacement, P1 strain, and P2 strain maps of a control subject (a–c) and of a LCBC patient (d–f), respectively.
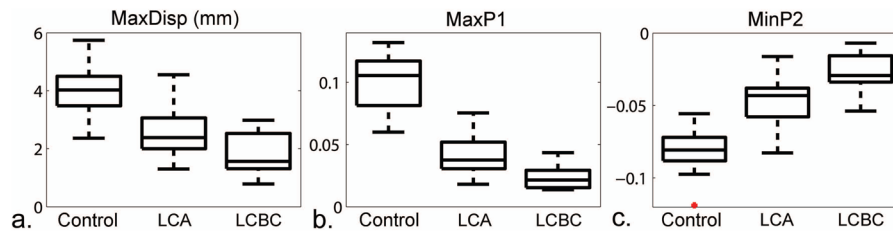
Figure 3.
Boxplots of: (a) maximum displacement (MaxDisp), (b) maximum P1 strain (MaxP1) and (c) minimum P2 strain (MinP2) for the control group, LCA patient group and LCBC patient group ($p < 0.05$ for all).
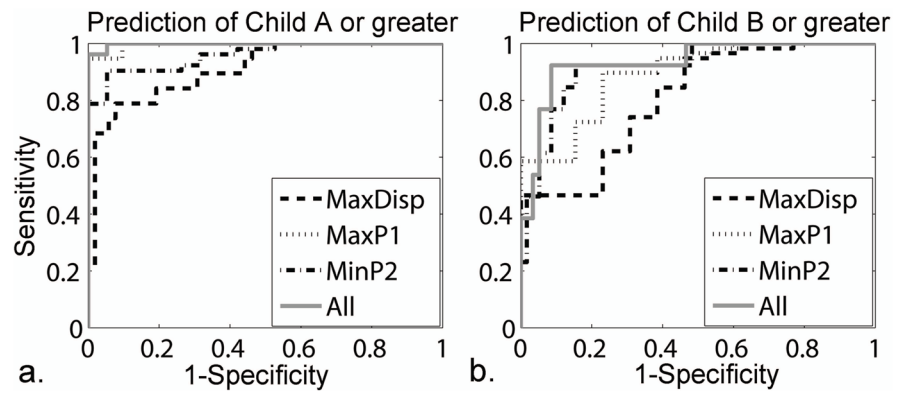
Figure 4.
ROC curves (a) for prediction of Child-Pugh A or greater and (b) for prediction of Child-Pugh B or greater, with MaxDisp, MaxP1, MinP2 and combination of all measures.

Table 1

Demographics for All Three Groups and Clinical Parameters in Patients with Liver Cirrhosis

	Control (n = 19)	LCA (n = 39)	LCBC (n = 13)
Age (y)	29.4 ± 5.2	58.4 ± 9.6	62 ± 9.1
Sex			
No. female	7	15	2
No. male	12	24	11
Body weight (kg)	65.5 ± 9.4	62.2 ± 10.7	64.5 ± 10.3
Total bilirubin (mg/dL)	x	0.9 ± 0.4	3.0 ± 4.0
Albumin (g/dL)	x	4.2 ± 0.4	2.9 ± 0.5
International normalized ratio	x	1.0 ± 0.1	1.2 ± 0.2
No. patients with ascites	x	2	10
No. of patient with hepatic encephalopathy	x	0	0
Child-Pugh score	x	5.1 ± 0.3	7.8 ± 1.1

Table 2

Summary of Liver Stiffness Measures in Control, LCA, LCBC Groups (Total n = 71)

Groups	MaxDisp (mm)	MaxP1	MinP2
Control	3.98 ± 0.88	0.10 ± 0.02	−0.08 ± 0.01
LCA	2.52 ± 0.73	0.04 ± 0.01	−0.05 ± 0.02
LCBC	1.86 ± 0.77	0.02 ± 0.01	−0.03 ± 0.01

Table 3

P-values of Group Comparisons for Each Measure, without and with Adjustment for Age and Gender. (P-values are shown without (Raw) and with (HSD) a Tukey's HSD multiple comparison correction.)

	Groups Compared		Not Adjusted For Age, Gender		Adjusted For Age, Gender	
			Raw	HSD	Raw	HSD
MaxDisp	Control	LCA	<0.0001	<0.0001	0.0071	0.0349
	LCA	LCBC	0.0079	0.0214	0.0040	0.0109
MaxP1	Control	LCA	<0.0001	<0.0001	<0.0001	<0.0001
	LCA	LCBC	<0.0001	<0.0001	<0.0001	0.0002
MinP2	Control	LCA	<0.0001	<0.0001	0.0002	0.0012
	LCA	LCBC	<0.0001	<0.0001	<0.0001	0.0002

Table 4

Areas Under the Receiver Operating Characteristics Curve (AUC) and Maximized Sensitivity and Specificity for Quantification of Liver Stiffness (Total n = 71)

	Prediction of Child A or Greater			Prediction of Child B or Greater		
	AUC	Sensitivity	Specificity	AUC	Sensitivity	Specificity
MaxDisp	0.910	94.2 %	73.7 %	0.806	61.5 %	82.8 %
MaxP1	0.995	98.1 %	94.7 %	0.891	76.9 %	86.2 %
MinP2	0.959	90.4 %	78.9 %	0.916	76.9 %	91.4 %
All*	0.998	98.1 %	94.7 %	0.934	92.3 %	87.9 %

*Combination of liver stiffness measures of MaxDisp, MaxP1, and MinP2.